ADVANCED FUNCTIONAL MATERIALS
www.afm-journal.de

Design and Synthesis of Multifunctional Drug Carriers Based on Luminescent Rattle-Type Mesoporous Silica Microspheres with a Thermosensitive Hydrogel as a Controlled Switch

Xiaojiao Kang, Ziyong Cheng, Dongmei Yang, Ping'an Ma, Mengmeng Shang, Chong Peng, Yunlu Dai, and Jun Lin**

A novel approach for the fabrication of multifunctional microspheres integrating several advantages of mesoporous, luminescence, and temperature responses into one single entity is reported. First, the hollow mesoporous silica capsules are fabricated via a sacrificial template route. Then, Gd_2O_3:Eu^{3+} luminescent nanoparticles are incorporated into the internal cavities to form rattle-type mesoporous silica nanocapsules by an incipient-wetness impregnation method. Finally, the rattle-type capsules serve as a nanoreactor for successfully filling temperature-responsive hydrogel via photoinduced polymerization to form the multifunctional composite microspheres. The organic–inorganic hybrid microspheres show a red emission under UV irradiation due to the luminescent Gd_2O_3:Eu^{3+} core. The in vitro cytotoxicity tests show that the samples have good biocompatibility, which indicates that the nanocomposite could be a promising candidate for drug delivery. In addition, flow cytometry and confocal laser scanning microscopy (CLSM) confirm that the sample can be effectively taken up by SKOV3 cells. For in vitro magnetic resonance imaging (MRI), the sample shows the promising spin-lattice relaxation time (T_1) weighted effect and could potentially apply as a T_1-positive contrast agent. This composite drug delivery system (DDS) provides a positive temperature controlled "on-off"drug release pattern and the drug, indomethacin (IMC), is released fast at 45 °C (on phase) and completely shut off at 20 °C (off phase). Meanwhile Gd_2O_3:Eu^{3+} plays an important role as the luminescent tag for tracking the drug loading and release process by the reversible luminescence quenching and recovery phenomenon. These results indicate that the obtained multifunctional composite has the potential to be used as a smart DDS for biomedical applications.

1. Introduction

Compared with conventional mesoporous silica materials, such as MCM-41 (Mobil Composition of Matter No. 41), SBA-15 (Santa Barbara amorphous silica-15), and MCF (siliceous mesocellular foam), hollow mesoporous silica spheres have attracted considerable attention for drug and gene delivery due to the fact that they can provide a higher storage capacity and exhibit sustained drug release kinetics.[1] Moreover, particles with spherical morphology are favorable for drug delivery because of their injectable and ingestible properties.[2] Recently, lanthanide-doped luminescent materials have become a hot subject of research as a new class of luminescent optical labels in biological assays and medical imaging.[3] Notably, gadolinium oxide doped with europium ions (Gd_2O_3:Eu^{3+}) has been proven to be an important red-emitting phosphor as a result of its good optical properties, high chemical and photochemical stability, and low toxicity.[4] Furthermore, Gd^{3+} is commonly used as a positive contrast agent for magnetic resonance imaging (MRI) in current clinical applications.[5] Hence, Gd_2O_3:Eu^{3+} can work as bimodal imaging probe of optical imaging and MRI. Therefore, synthesis of rattle-type structure of a mesoporous shell and movable core with an interstitial hollow space between them is an effective strategy to combine the merits of the high drug payload of hollow mesoporous silica spheres and the biolabel function of luminescent particles.[6]

In recent years, much effort has been dedicated to the development of "smart" drug delivery systems (DDSs) because the drug entrapped into the carriers can be released in a controlled way at specific time intervals at a required site in response to external stimulation, such as temperature, pH, magnetic field, ultrasound, ion strength.[7] Poly(*N*-isopropylacrylamide) (PNIPAm), the most extensively investigated temperature-sensitive

Dr. X. Kang, Dr. Z. Cheng, Dr. D. Yang, Dr. P. Ma, Dr. M. Shang, Dr. C. Peng, Dr. Y. Dai, Prof. J. Lin
State Key Laboratory of Rare Earth Resource Utilization
Changchun Institute of Applied Chemistry
Chinese Academy of Sciences
Changchun, 130022, P. R. China
E-mail: zycheng@ciac.jl.cn; jlin@ciac.jl.cn
Dr. X. Kang, Dr. D. Yang, Dr. M. Shang, Dr. C. Peng, Dr. Y. Dai, Prof. J. Lin
Graduate University of the Chinese Academy of Sciences
Beijing, 100049, P. R. China

DOI: 10.1002/adfm.201102746

polymer, exhibits a reversible phase transition at the lower critical solution temperature (LCST, 32 °C) in aqueous solution.[8] Below the LCST, the polymer is expanded and soluble, whereas it is collapsed and insoluble when heated above the LCST.[9] Since the temperature is intermediate between room temperature and body temperature, PNIPAm has been widely used as a drug carrier.[10] Generally, PNIPAm hydrogel affords a negative temperature release, via a skin layer regulated diffusion mechanism.[11] At the temperature above the LCST, PNIPAm hydrogel may shrink and quickly form a dense, thick skin layer and block off the drug release. With a temperature decrease, the hydrogel network expands to increase the mesh size and allows drug molecules to diffuse out, which leads to an increase in the drug release rate. However, in some cases, a positive controlled release pattern, i.e., the faster drug release at increased temperature, is expected because it can respond to an increased body temperature arising from diseases such as inflammation or cancers.[12] In a positive controlled pattern, an already hydrated gel collapsed rapidly when heated, exuding water and much of the imbedded drug. In recent years, remarkable progress has been made in developing hyperthermia for disease therapy, in particular tumor treatment. Some external fields energy, such as magnetic fields, near-infrared (NIR) laser, and ultrasonication, can penetrate through deep tissue and rapidly improve the regional temperature to achieve localized therapy.[13] The positive thermal-sensitive hydrogel is an ideal DDS in combination with hyperthermia for triggering drug release. Unfortunately, in positive released hydrogels it is difficult to realize the off-phase for drug release when it swells at low temperature, which greatly limits their practical applications. Therefore, a rational design for developing a positive intelligent DDS is still urgently needed to meet the requirements.

Here, we design and synthesize P(NIPAm-*co*-AAm) hydrogel-modified luminescent rattle-type mesoporous silica microspheres, where AAm is acrylic acid amide. The rattle-type structure was obtained by incorporating Gd_2O_3:Eu^{3+} luminescent particles into the hollow mesoporous silica microspheres via an incipient-wetness impregnation route. Subsequently, the monomers of the hydrogel were impregnated into the interstitial space of microrattles and applied photoinduced polymerization. Thus the temperature-sensitive hydrogel was successfully filled into the middle layer and the channels of the mesoporous silica. As far as we known, most research work is done on coating or grafting thermosensitive PNIPAm onto the exterior surface of mesoporous silica particles.[14] Polymerization of PNIPAm-based hydrogel into the inner cavity of a rattle-type mesoporous silica spheres is rarely reported. The design of the unique architecture is in order to confine the soft hydrogel within the rigid silica shells and the mesochannels were expected to be blocked off at low temperature with hydrogel swelling. At high temperature, the mesochannels were opened with the shrinking of polymer gel and the entrapped drugs were squeezed out depending on a positive release mechanism.[15] Moreover, the PNIPAm-based hydrogel is very fragile owing to the poor mechanical properties, which greatly limits its practical applications.[16] Encapsulation of PNIPAm hydrogel in the rigid silica rattles is in favor of preventing the fragments leaking out and therefore improving the safety performance when they are used as a DDS in human body. Additionally, compared with the other synthetic methods, such as atom transfer radical polymerization (ATRP) and reversible addition-fragmentation chain transfer (RAFT) polymerization for preparation of PNIPAm-based composites, photoinduced polymerization and crosslinking is a rather facile and time-saving strategy, and is convenient for incorporating other functional monomers, such as AAm in this paper.[14c,16a] Finally, the in vitro MTT assays show that the as-prepared composite carriers have good biocompatibility, which indicates that the novel nanocomposite could be a promising candidate for drug delivery. Cell uptake of composite by SKOV3 cells was examined by flow cytometry and confocal laser scanning microscope (CLSM). Because of the Gd^{3+} ions in the composites, these microspheres can act as a spin-lattice relaxation time (T_1)-MR contrast agent. Indomethacin (IMC), a non-steroidal anti-inflammatory drug commonly used to reduce fever, pain, stiffness, and swelling, was selected to study drug release of the composite carrier. The loading amount of the drug (IMC) reached as high as 28.6 wt%, and the release behavior of IMC was obviously temperature dependent. The rapid drug release behavior at 45 °C and stopping of release at 20 °C was found, indicating that we can regulate the rate of drug release via the change of the temperature due to the unique architecture of composite carriers and controlled switching of hydrogel.

2. Results and Discussion

2.1. Preparation and Characterization of Gd_2O_3:Eu^{3+}@P(NIPAm-co-AAm)@HMS Microspheres

Scheme 1 illustrates the procedure for the synthesis of Gd_2O_3:Eu^{3+}@P(NIPAm-co-AAm)@HMS microspheres and subsequently loading and release of IMC in the present work. Firstly, the pre-formed Fe_3O_4 particles were coated with mesoporous silica layer by the hydrolysis and condensation of tetraethoxysilane (TEOS)and cetyltrimethylammonium bromide (CTAB) was used as templating agent (Figure S1 and S2, Supporting Information). Then, removing the templates involved extracting CTAB with acetone and etching the Fe_3O_4 core with HCl solution to form the hollow mesoporous silica (HMS) nanocapsules. Next, the transparent precursor solution containing gadolinium nitrate and europium nitrate aqueous solution was impregnated into the HMS with the aid of vacuum suction owing to the wetting action and the capillary force. The vacuum conditions favor removal of the air inside HMS. The precursor-containing HMS was calcined at 550 °C in order to obtain rattle-like Gd_2O_3:Eu^{3+}@HMS. Finally, the as-prepared rattle-type capsules served as a nanoreactor for successfully filling temperature-responsive P(NIPAm-*co*-AAm) hydrogel via photoinduced polymerization to form the multifunctional composite microsphere, denoted as Gd_2O_3:Eu^{3+}@P(NIPAm-*co*-AAm)@HMS. Furthermore, IMC was used as a model drug to assess the drug loading and controlled release of the composite carriers.

Figure 1 shows representative scanning electron microscopy (SEM) (Figure 1a,b) and transmission electron microscopy (TEM) (Figure 1c,d) images of the HMS samples prepared using Fe_3O_4 as a hard template. The HMS microspheres have a smooth surface with a mean diameter of 400 nm, as determined

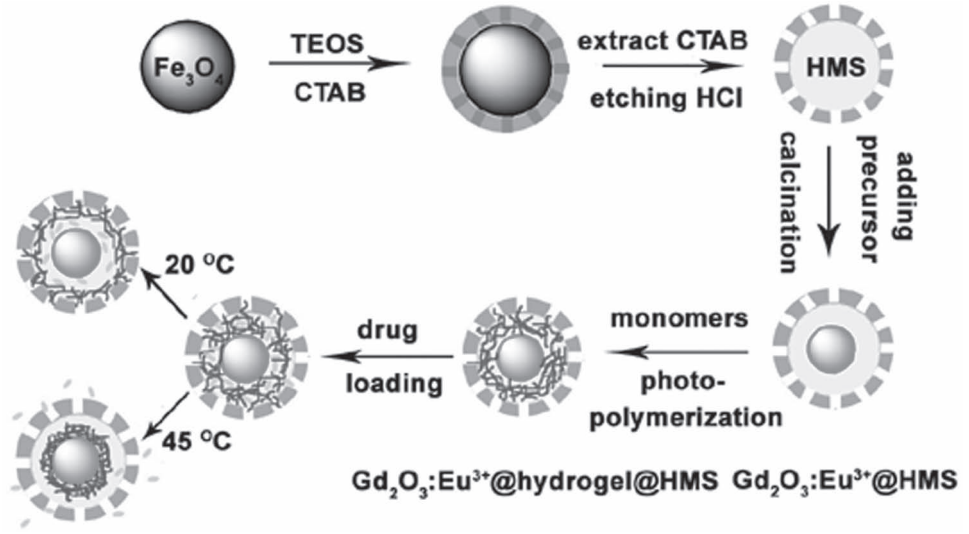

Scheme 1. Scheme for the synthetic process for P(NIPAm-co-AAm) hydrogel modified luminescent rattle-type mesoporous silica microspheres and subsequent loading and temperature-controlled release of IMC.

from the SEM image (Figure 1a). The hollow structure can be confirmed by a selected broken microsphere under SEM observation (Figure 1b) and the wall thickness of the shell is around 50 nm. The TEM images (Figure 1c,d) of HMS also revealed that Fe_3O_4 templates have been etched out and the shell of the hollow silica microspheres presents the typical feature of mesoporous structure. The shells exhibited rather uniform thickness and the mesochannels penetrate from the surface to the inner cavity. Such a feature is highly desired for drug loading and transport.

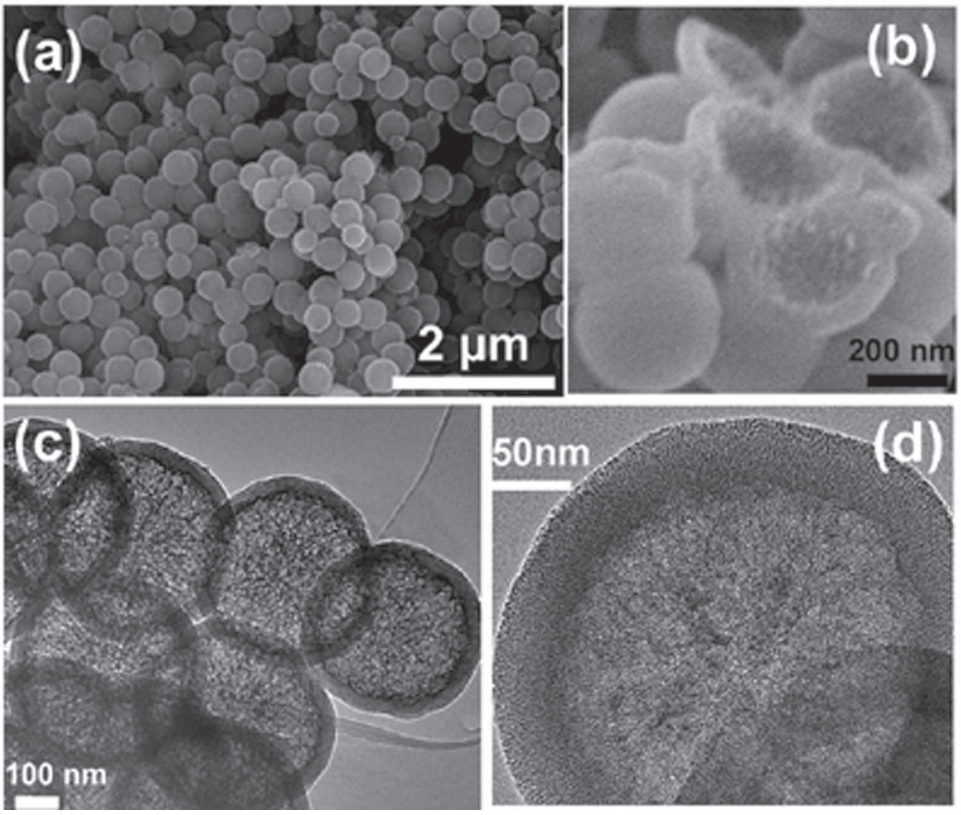

Figure 1. SEM and TEM images of HMS sample: a,b) low- and high-magnification SEM images and c,d) low- and high-magnification TEM images.

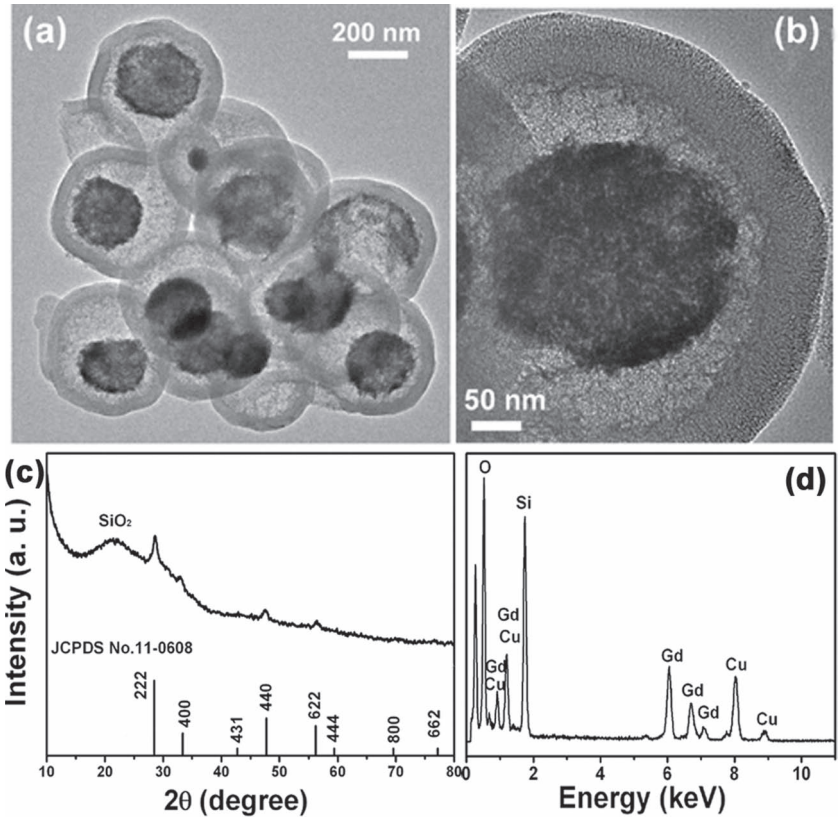

Figure 2. a,b) TEM images, c) XRD pattern, and d) EDX spectrum of as-prepared Gd_2O_3:Eu^{3+}@HMS sample.

A vacuum suction was employed during the experiments in order to impregnate the gadolinium nitrate and europium nitrate solutions into the cavity of the HMS. After calcinations in air, Gd_2O_3:Eu^{3+} particles crystallized in the cavity of HMS. In the TEM image (**Figure 2**a), the rattle-type structure can be clearly distinguished because of the difference of electron penetrability and image contrast between the cores and shells. Seen from the wide-angle X-ray diffraction (XRD) pattern (Figure 2c), the broad band located at $2\theta = 22°$ can be assigned to the characteristic diffraction peak of amorphous SiO_2 (JCPDS 29-0085), and the four diffraction peaks at 2θ= 28.5°, 34.1°, 47.8°, and 56.3° should be attributed to the crystallized Gd_2O_3:Eu^{3+} (JCPDS 11-0608). In addition, energy dispersive X-ray spectroscopy (EDX) data (Figure 2d) confirms the presence of silicon (Si), oxygen (O), gadolinium (Gd), and europium (Eu) in the as-prepared sample. On the basis of these results, it is believed that the void space of HMS is filled with functional Gd_2O_3:Eu^{3+} beads and formed the rattle-like structure.

Figure 3a displays the TEM image of the Gd_2O_3:Eu^{3+}@HMS samples after decorating with temperature-sensitive P(NIPAm-*co*-AAm) polymer. The mesoporous structure on the shell can still be observed clearly, and no bulk polymer can be seen from the external surface of the microspheres. The EDX elemental mapping was further carried out to identify the composition and the elemental distributions of Si, O, Gd, Eu, C, and N in the composite microspheres (Figure 3b–h). The Gd and Eu signals (Figure 3e,f) show that Gd_2O_3:Eu^{3+} particles were mainly mustered in the center of HMS and only a small quantity of Gd_2O_3:Eu^{3+} was deposited in the mesoporous channels of silica shell. And the widely distributed C and N signals confirm the successful polymerization of thermal-sensitive P(NIPAm-co-AAm) hydrogel within the middle layer or mesochannels.

The Fourier transform infrared (FTIR) spectra for HMS, Gd_2O_3:Eu^{3+}@HMS, Gd_2O_3:Eu^{3+}@P(NIPAm-co-AAm)@HMS, IMC-loaded Gd_2O_3:Eu^{3+}@ P(NIPAm-*co*-AAm)@HMS, and pure IMC are depicted in **Figure 4**, respectively. In the case of HMS (Figure 4a), the obvious absorption bands from

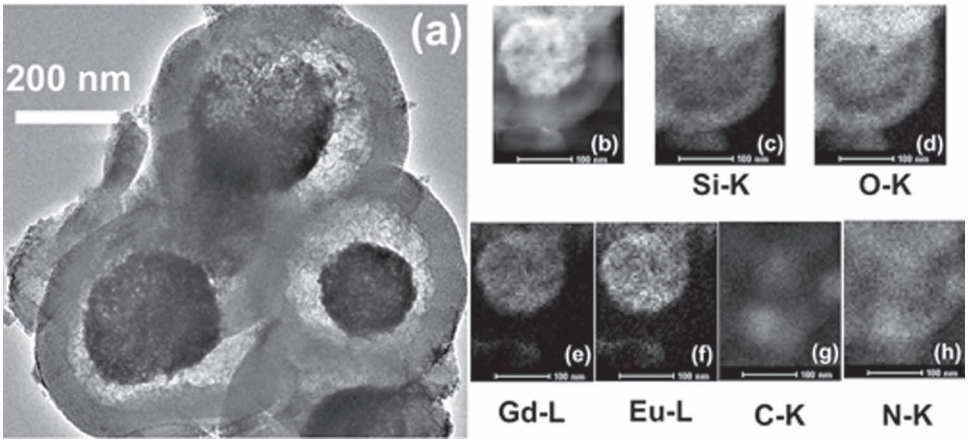

Figure 3. TEM image (a), high angle annular dark field scanning transmission electron microscopy (HAADF-STEM) image (b) and the corresponding 2D dimensional EDX elemental mapping for Si (c), O (d), Gd (e), Eu (f), C (g), and N (h) of Gd_2O_3:Eu^{3+}@P(NIPAm-*co*-AAm)@HMS composite microspheres.

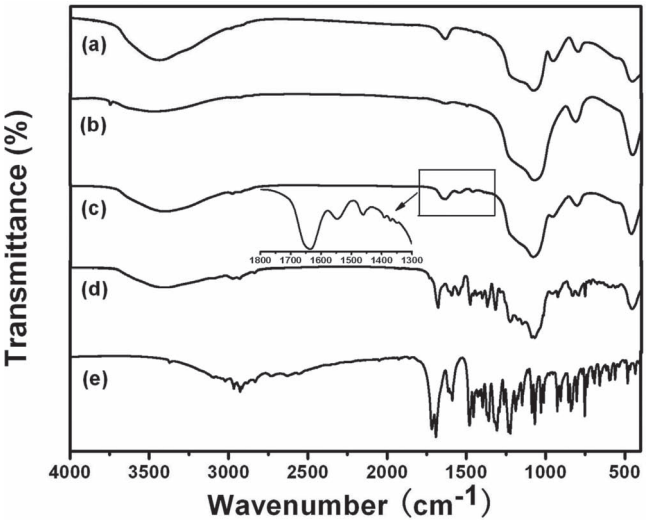

Figure 4. FTIR spectra of HMS (a), Gd_2O_3:Eu^{3+}@HMS (b), Gd_2O_3:Eu^{3+}@P(NIPAm-co-AAm)@HMS (c), IMC-loaded Gd_2O_3:Eu^{3+}@P(NIPAm-co-AAm) @HMS (d), and pure IMC (e).

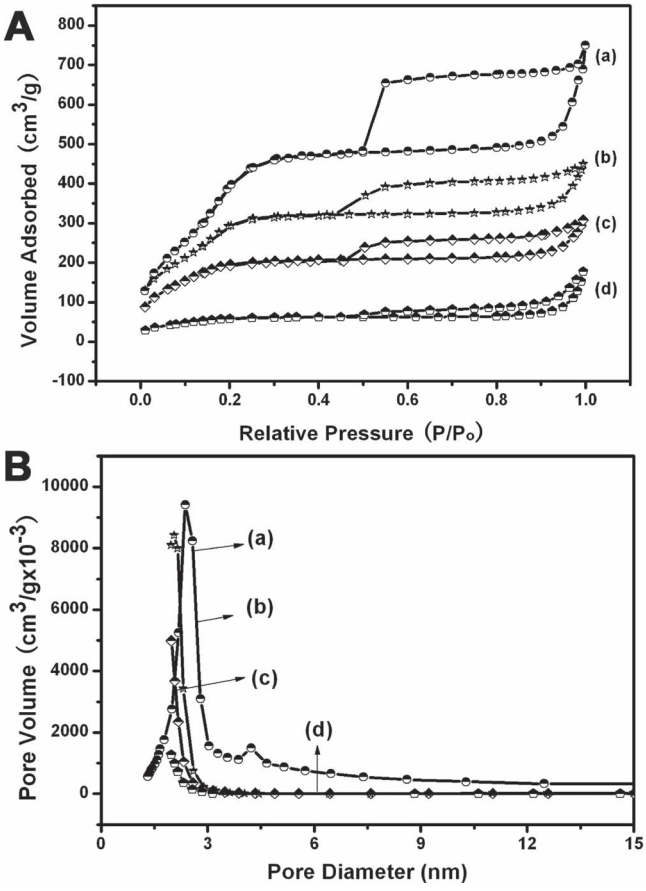

Figure 5. N_2 adsorption/desorption isotherms (A) and the corresponding pore sized distributions (B) for HMS (a), Gd_2O_3:Eu^{3+}@HMS (b), Gd_2O_3:Eu^{3+}@P(NIPAm-*co*-AAm)@HMS (c), and IMC-loaded Gd_2O_3:Eu^{3+}@P(NIPAm-*co*-AAm)@HMS (d).

OH (3450 cm^{-1}), H_2O (1635 cm^{-1}), Si–O–Si (ν_s, 1080 cm^{-1}; ν_{as}, 803 cm^{-1}), Si–OH (ν_s, 951 cm^{-1}), and Si–O (δ, 469 cm^{-1}) (where ν_s represents symmetric stretching, ν_{as} asymmetric stretching, and δ bending) are present.[17] Compared with that of HMS, the intensity of the OH and Si–OH groups decreased due to calcination for introducing Gd_2O_3:Eu^{3+} crystal. In Figure 4c, the appearance of characteristic IR peaks at 1649 and 1548 cm^{-1} in Gd_2O_3:Eu^{3+}@P(NIPAm-*co*-AAm)@HMS should be attributed to the C=O stretching and N–H bending vibrations, respectively. In addition, the band at 1456 cm^{-1} corresponds to the bending vibration of C–H while the bands at 1386 and 1367 cm^{-1} are attributed to isopropyl group. These results indicate that P(NIPAm-*co*-AAm) was successfully incorporated into Gd_2O_3:Eu^{3+}@HMS sample. Furthermore, two main characteristic bands at 1724 and 1691 cm^{-1} in pure IMC (Figure 4e) can be assigned to the stretching vibration bands of aliphatic and aromatic carbonyl groups, respectively. After loading into P(NIPAm-*co*-AAm) modified carriers, the IR band of IMC at 1691 cm^{-1} appeared to shift to a lower wavenumber of 1680 cm^{-1}, which may be explained by the interaction of this carbonyl group with the amide groups of P(NIPAm-*co*-AAm).

Figure 5A shows the N_2 adsorption-desorption isotherms of HMS, Gd_2O_3:Eu^{3+}@HMS, Gd_2O_3:Eu^{3+}@P(NIPAm-co-AAm)@HMS, IMC-loaded Gd_2O_3:Eu^{3+}@P(NIPAm-*co*-AAm)@ HMS and their corresponding pore size distributions are shown in Figure 5B. The isotherms of all the samples can be classified as type IV with the leap start-points at relative pressures of P/P_0 = 0.2–0.3, which demonstrates the typical ordered mesoporous structure. In addition, all the samples exhibited H4 hysteresis loops, which have conventionally been associated with narrow slit-like pores. However, some reports indicate that hollow spheres with walls composed of ordered mesoporous silica also exhibited this type hysteresis behavior due to the delay of nitrogen evaporation from the hollow voids blocked by the surrounding mesopores in the shells during the N_2 desorption process.[1g,18] It can be clearly seen from Figure 5A that the proportion of hysteresis loop shrinks gradually with loading of Gd_2O_3:Eu^{3+}, P(NIPAm-co-AAm) and IMC due to the occupancy of internal void. Meanwhile, all the samples have narrow pore distributions and the pore size distribution peaks, as expected, shift toward smaller pore diameter. The structure parameters of these four samples are given in **Table 1**. It can be seen that HMSs possess a relatively high Brunauer–Emmett–Teller (BET) surface area of 1465 m^2 g^{-1} and a pore volume of 1.28 cm^3 g^{-1}, making these microspheres an ideal host for loading guest species of diverse sizes, shape, and functionalities. Additionally, the BET surface area and pore volume decrease after modification of Gd_2O_3:Eu^{3+} and P(NIPAm-*co*-AAm) and further incorporation of IMC. It is worthwhile to point out that the obtained multifunctional microspheres with mesoporous, luminescent, and temperature-sensitive properties still have moderate BET surface area and pore volume for storing drug molecules because of their unique mesoporous rattle-type structure.

Figure S3 (Supporting Information) shows the low-angle XRD patterns of as-prepared HMS, Gd_2O_3:Eu^{3+}@HMS, Gd_2O_3:Eu^{3+}@P(NIPAm-*co*-AAm)@HMS and IMC-loaded Gd_2O_3:Eu^{3+}@P(NIPAm-*co*-AAm)@HMS, respectively. The (100)

Table 1. Textural properties of HMS, Gd_2O_3:Eu^{3+}@HMS, Gd_2O_3:Eu^{3+}@P(NIPAm-*co*-AAm) @HMS and IMC-loaded Gd_2O_3:Eu^{3+}@P(NIPAm-*co*-AAm)@HMS samples.

Samples	V_p [a)] [$cm^3\ g^{-1}$]	S_{BET} [b)] [$m^2\ g^{-1}$]	D_p [c)] [nm]	IMC loading [wt.%]
HMS	1.28	1465	3.50	
Gd_2O_3:Eu^{3+}@HMS	0.61	1057	2.68	
Gd_2O_3:Eu^{3+}@P(NIPAm-*co*-AAm)@HMS	0.41	662	2.47	
IMC-loaded Gd_2O_3:Eu^{3+}@P(NIPAm-*co*-AAm)@HMS	0.17	198	2.01	40.3

[a)] Pore volume; [b)] Surface area calculated using the Brunauer–Emmett–Teller (BET) method; [c)] The abbreviation for pore diameter.

and (110) Bragg diffraction peaks of the HMS sample can be observed (Figure S3a, Supporting Information), which is typical for ordered 2D hexagonal mesostructure (*P*6mm). The peak intensities of the Gd_2O_3:Eu^{3+} encapsulated, P(NIPAm-*co*-AAm) modified, and IMC-loaded samples decrease with respect to that of pure HMS, which can be attributed to the decrease of the mesoscopic order along with integrating functional materials and drug.

The photoluminescence (PL) properties of the Gd_2O_3:Eu^{3+}@P(NIPAm-co-AAm)@HMS sample were characterized by excitation and emission spectra (**Figure 6**). The excitation spectrum was taken with a monitoring wavelength of 610 nm and the emission spectrum was excited on 228 nm, respectively. The excitation spectrum consists of a broad intense band with a maximum at 228 nm and a shoulder at 249 nm, which could be attributed to the Gd_2O_3 host excitation band and charge-transfer absorption between the O^{2-} and Eu^{3+}, respectively.[19] After dispersing in water, the sample forms a translucent colloidal solution as seen under daylight (Figure S4a, Supporting Information). Upon excitation into the Gd_2O_3 host absorption band at 228 nm, the water-dispersed composite microspheres show red luminescence, which can

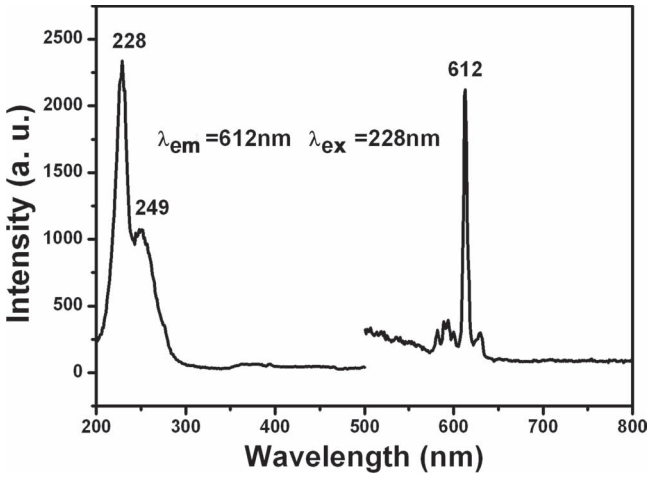

Figure 6. PL excitation (left, λ_{em} = 612 nm) and emission (right, λ_{ex} = 228 nm) spectra of Gd_2O_3:Eu^{3+}@P(NIPAm-*co*-AAm)@HMS.

be seen from the digital luminescence photograph taken under the irradiation of a 254 nm UV lamp (Figure S4b, Supporting Information). In the emission spectrum, the characteristic transition lines from the lowest excited $^5D_0$ level of Eu^{3+} to ^7F_J (J = 0, 1, 2) are observed, dominated by the Eu^{3+} $^5D_0 \rightarrow {}^7F_2$ transition, which is an electric-dipole-allowed transition and is hypersensitive to the environment.

2.2. In Vitro Cytotoxicity of Gd_2O_3:Eu^{3+}@P(NIPAm-*co*-AAm)@HMS Microspheres

It is important to evaluate the biocompatibility of a material for its potential biomedical applications. 3-(4,5-dimethylthiazol-2-yl)-2,5-diphenyltetrazolium bromide (MTT) assays were performed on L929 cell lines to evaluate the cytotoxicity of our samples. It can be seen from **Figure 7** that HMS, Gd_2O_3:Eu^{3+}@HMS and Gd_2O_3:Eu^{3+}@P(NIPAm-*co*-AAm)@HMS showed no significant cytotoxic effect on the L929 cells at 3.125–200 μg mL^{-1} after incubation for 24 h. Even the concentration of Gd_2O_3:Eu^{3+}@P(NIPAm-*co*-AAm)@HMS was as high as 200 μg mL^{-1}, the cell viability remained 96%. The results demonstrated that the obtained organic–inorganic composites are biocompatible and can be potentially used as the drug carriers.

2.3. Cell Uptake and In Vitro MR Imaging

The Gd_2O_3:Eu^{3+}@P(NIPAm-*co*-AAm)@HMS was labeled with fluorescent dye, fluorescein isothiocyanate (FITC), so the cell uptake degree of the composites could be quantified with flow cytometry by determining the green fluorescence emitted from Gd_2O_3:Eu^{3+}@P(NIPAm-*co*-AAm)@HMS-FITC treated SKOV3 cells. After incubation of SKOV3 cells with the sample for different times (10 min, 30 min, and 3 h), the cell-labeling ability of Gd_2O_3:Eu^{3+}@P(NIPAm-*co*-AAm)@HMS-FITC composites was estimated by flow cytometry. As revealed by **Figure 8**, Gd_2O_3:Eu^{3+}@P(NIPAm-*co*-AAm)@HMS-FITC composites were taken up by SKOV3 cells compared to the controlled cells, and the cell uptake of sample increases with incubation time.

To further verify the location of the particles relative to the cells, the confocal laser scanning microscopy (CLSM) photographs of human SKOV3 ovarian cancer cells incubated with FITC-labeled Gd_2O_3:Eu^{3+}@P(NIPAm-*co*-AAm)@HMS for 10 min, 30 min, and 3 h at 37 °C are showed in **Figure 9**. The green fluorescence of FITC can be clearly seen in confocal images with an excitation wavelength of 488 nm. In the first 10 min, the green FITC appears localized as scattered dots, which demonstrate that only a few of composites were taken up by SKOV3 cells. With the increase of the incubation time, the intensities of green signal increase, that is, more particles have crossed the membrane and localized in the cytoplasm. The results confirm that as-prepared samples can be effectively taken up by SKOV3 cells.

The Gd-containing composites have potential as a MR contrast agent due to their signal-enhancement ability. We evaluated in vitro spin-lattice relaxation time (T_1)-weighted images at 1.5 T for Gd_2O_3:Eu^{3+}@P(NIPAm-*co*-AAm)@HMS sample in

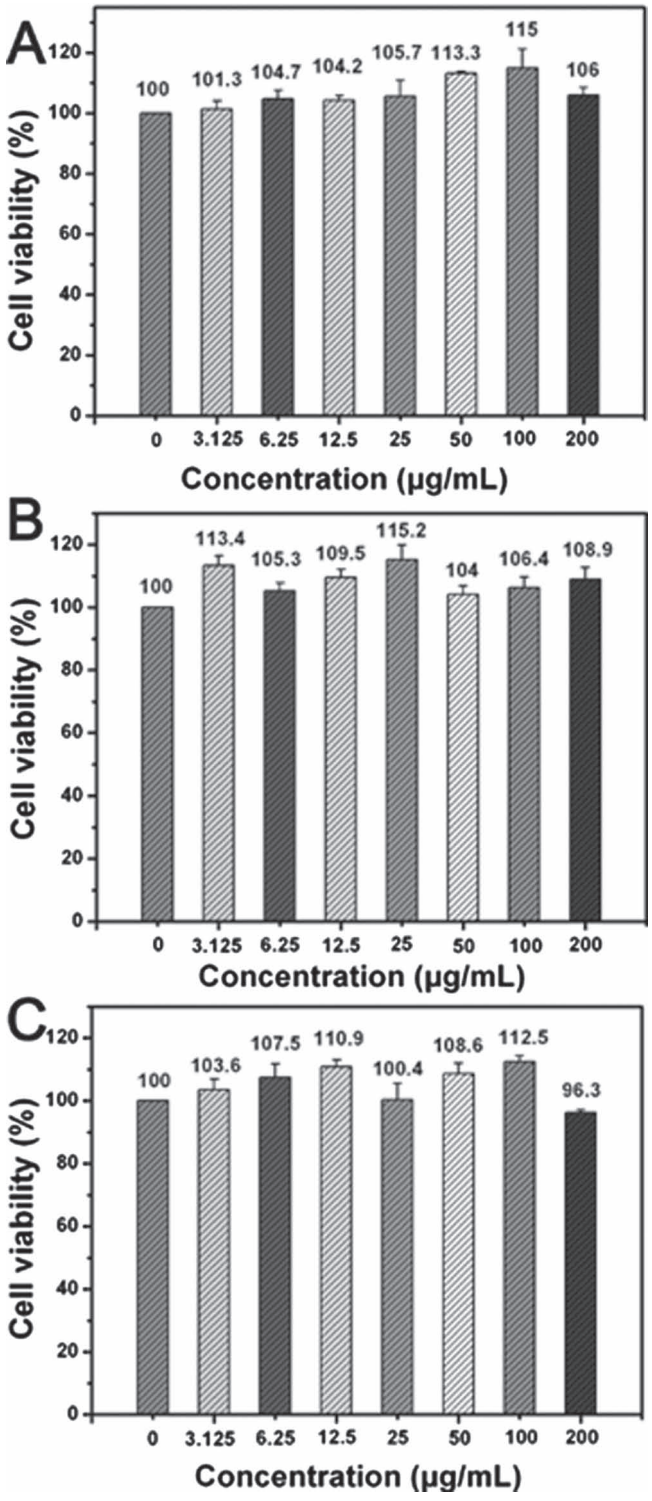

Figure 7. Cell viabilities of HMS, Gd_2O_3:Eu^{3+}@HMS and Gd_2O_3:Eu^{3+}@P(NIPAm-*co*-AAm)@HMS to L929 fibroblast cells measured by MTT assay.

the range of 0–0.75 mg mL^{-1} (**Figure 10**). With the increase of composites concentration, T_1-weighted MR imaging intensity substantially brightened, demonstrating that the sample could serve as T_1-MR contrast agent.

2.4. Drug Loading and Release Properties

Quantitative determination of the organic content was performed by TG analyses (Figure S5, Supporting Information). As shown from Figure S5 (Supporting Information), no notable decrease in weight can be observed for Gd_2O_3:Eu^{3+}@HMS in the temperature range from 25 to 800 °C. For the organic–inorganic composites of Gd_2O_3:Eu^{3+}@P(NIPAm-*co*-AAm)@HMS, however, a high decrease of 13.9% in weight is found, indicating that the polymer content is about 13.9 wt% in the composite (Figure S5b, Supporting Information). Furthermore, the loading amount of drug is calculated by the difference of weight loss between the dried Gd_2O_3:Eu^{3+}@P(NIPAm-*co*-AAm)@HMS and IMC-loaded Gd_2O_3:Eu^{3+}@P(NIPAm-*co*-AAm)@HMS. As a result, the payload of IMC in the composite microspheres is determined to be 400 mg IMC per Gd_2O_3:Eu^{3+}@P(NIPAm-*co*-AAm)@HMS g. Although the porous volume and surface area decreased greatly after integrating the functional materials into HMS, the rattle-type composite carriers still possess a high drug storage capacity.

The release behavior of IMC from the Gd_2O_3:Eu^{3+}@P(NIPAm-*co*-AAm)@HMS composites in 10 mM phosphate buffered saline (PBS) buffer in response to a temperature change between 20 and 45 °C is shown in **Figure 11**A. As can be seen, besides an initial small burst effect due to the presence of the drug at the surface, the drug release was completely cut off and even exhibited a slight negative release rate at the low temperature (20 °C), whereas the system showed a sustained release behavior at 45 °C. The "turn on" and "turn off" phase of drug release is cycled by the changes of temperature. In contrast, there is no significant change of the IMC release rate observed between 20 and 45 °C by using Gd_2O_3:Eu^{3+}@HMS as carrier, in which the thermal-sensitive hydrogel is absent (Figure 11B). These results implied that the temperature-sensitive hydrogel play an important role of controlled switch for drug release. We suppose that hydrogel absorbs water and expands in a great extent in the cool medium (20 °C), however, the swelling was confined to the rigid silica shell, which brings about a consequence that the cavity and channels were stuffed with the swelling hydrogel network and blocked the drug release to a certain extent. On the other hand, as the temperature is increased above the LCST of P(NIPAm-*co*-AAm), the shrinking of the hydrogel opened the porous channels and simultaneously squeezed out the drug molecules entrapped into the hydrogel network. Swelling and deswelling of polymer gel by changing temperature is similar to a physical squeezing and water reabsorption of a sponge. In other words, the temperature-responsive P(NIPAm-*co*-AAm) works like a thermopump that squeezes and sucks up media utilizing its reversible phase transition. In addition, based on the previous study, the integrating of hydrophilic monomer of AAm into PNIPAM gel can effectively improve the water content, response rate to temperature changes, and improve the LCST of the PNIPAm hydrogel.[20] This should be attributed to the hydrophilic AAM is considered as the diffusion channels for water molecules and prevent the forming of the dense skin layer at the external surface of hydrogel at high temperature. However, besides temperature, the phase transition behavior of PNIPAm is also affected by many factors, such as salt concentrations or surfactants in media. Some published reports

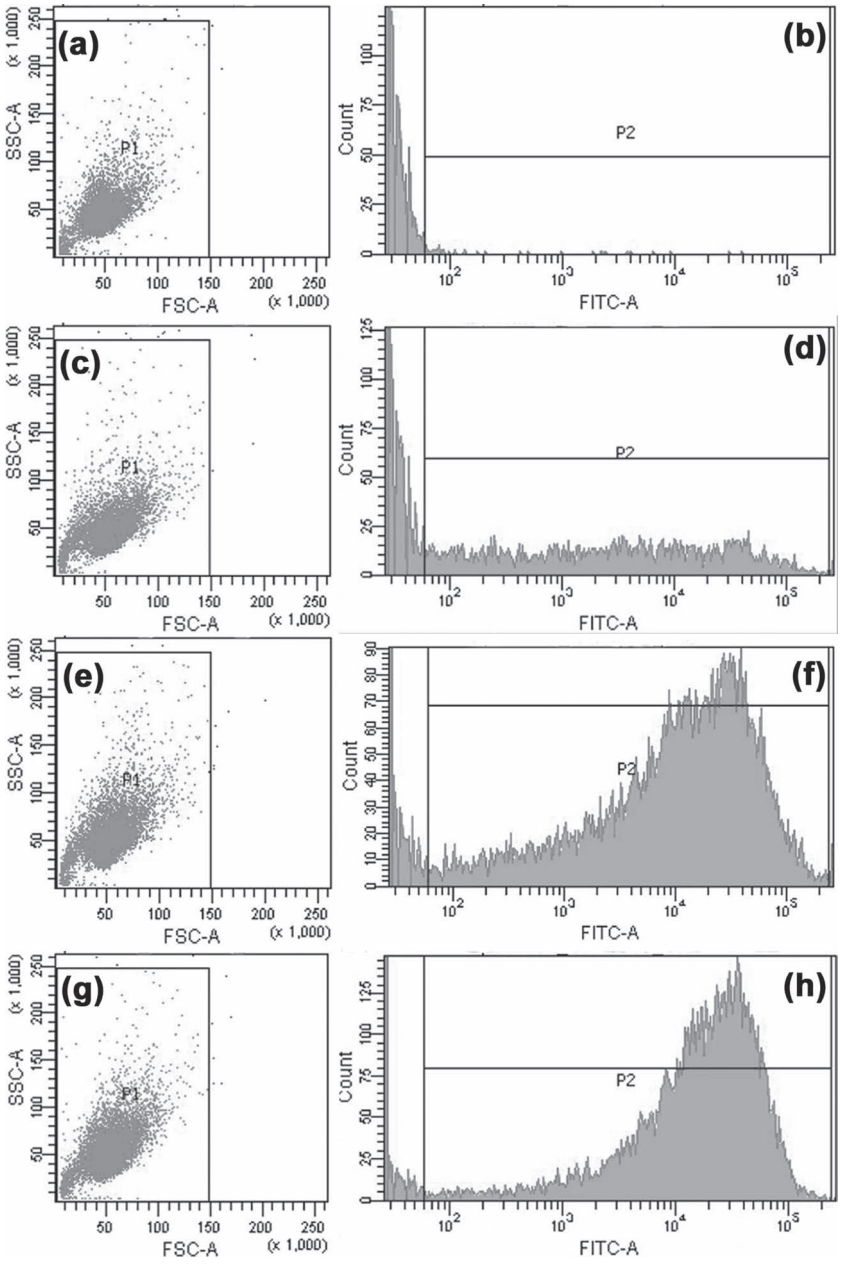

Figure 8. Flow cytometry analysis of the control cells (a,b) and SKOV3 cells incubated with Gd_2O_3:Eu^{3+}@P(NIPAm-*co*-AAm)@HMS-FITC composites for 10 min (c,d), 30 min (e,f), and 3 h (g,h).

indicated that the presence of salt in solution can shift LCST and influence the stability of PNIPAm due to the direct interactions between the salt ions and the polymer.[21] The salts could destroy the hydration structures and subsequent aggregation of PNIPAm. This "salting out effect" phenomenon is observed in many different kinds of biological buffers. Hence, the thermosensitive behavior of PNIPAm become relative complicated in a practical bioenvironment. It still requires detailed investigation to improve our prepared drug carrier and resolve aforementioned problem.Figure 11. Controlled release of IMC from Gd_2O_3:Eu^{3+}@P(NIPAm-*co*-AAm)@HMS (A) and Gd_2O_3:Eu^{3+}@HMS (B) in response to temperature changes in 10 mM PBS (pH = 7.4). C) PL emission intensity of Eu^{3+} in Gd_2O_3:Eu^{3+}@P(NIPAm-*co*-AAm)@HMS as a function of the cumulatively released IMC.

We also investigated the relationship between PL intensity of the IMC-loaded Gd_2O_3:Eu^{3+}@P(NIPAm-*co*-AAm)@HMS and the cumulative release of drug. As shown in Figure 11C, the emission intensity of Gd_2O_3:Eu^{3+} was completely quenched after loading IMC and subsequently underwent a recovery process with a continued release of drug. It is well known that the emission of rare earth ions will be quenched to some extent in the environments where high phonon frequencies are present. The organic groups in IMC with tremendous vibration frequencies from 1000 and 3200 cm^{-1} will quench the emission of Eu^{3+} to a great extent. According to previous reports, it is found that the radiative rate is approximately equal to the non-radiative rate if the energy gap in the non-radiative transition equals five times the maximum phonon frequency.[22] In IMC-loaded luminescent microspheres, the maximum phonon energy of IMC is about 3100 cm^{-1} (determined by the IR spectra shown in Figure 4d) and the energy gaps between the $^5D_0$ and $^7F_5/^7F_4/^7F_3$ levels amount to 13 453/14 508/15 486 cm^{-1}, respectively. These energy gaps are smaller than five times of the maximum phonon energy of IMC (3100 cm^{-1}). Hence, the relaxation of the excited electrons from $^5D_0$ level to the lower $^7F_5/^7F_4/^7F_3$ levels is liable to occur due to IMC molecules in our system, resulting in the decrease of red emission from $^5D_0$ level. With the increase of release time, more and more IMC molecules can be liberated from system and the quenching effect would be weakened, resulting in the increase of emission intensity. This property makes the drug delivery system can be easily identifiable and monitorable during the drug release process.

3. Conclusions

In summary, we have demonstrated a feasible route to the synthesis of multicompartment drug carrier containing a luminescent rattle-type mesoporous silica microsphere filled with the thermosensitive hydrogel as temperature-controlled switch. Distinctive of the conventional synthetic route, we first prepared the hollow mesoporous silica capsules via the sacrificial template route and followed that was used as a nanoreactor to fill the Gd_2O_3:Eu^{3+} and P(NIPAm-co-AAm) hydrogel. The organic–inorganic hybrid microspheres demonstrate a good biocompatibility by MTT assay in terms of in vitro cytotoxicity test to L929 cells. Flow cytometry

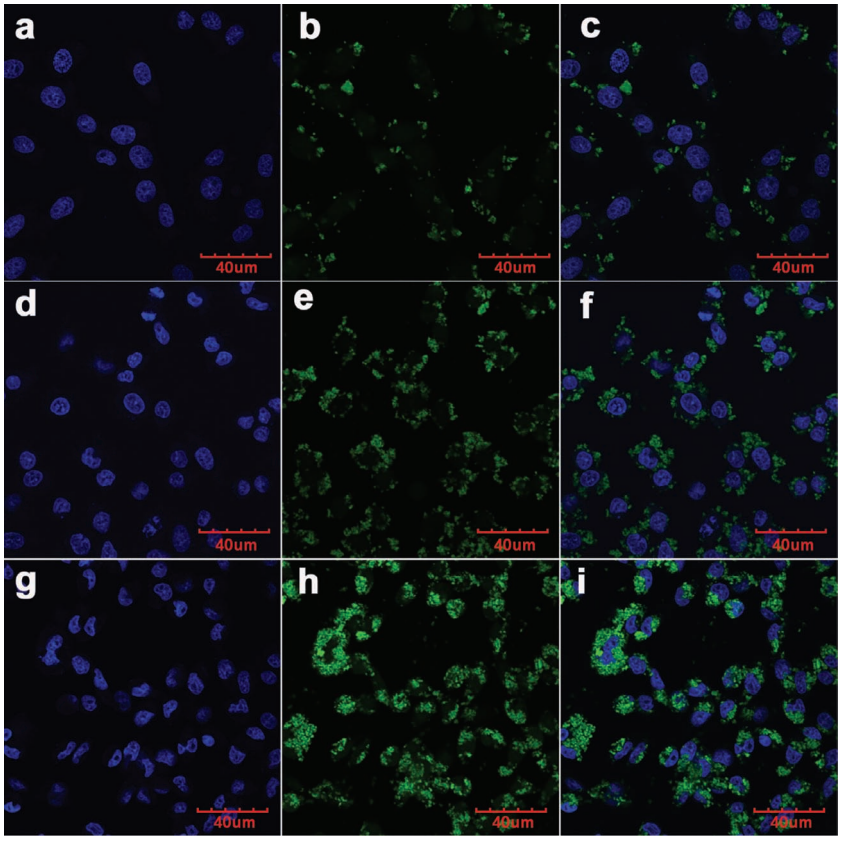

Figure 9. LCSM images of SKOV3 cells incubated with Gd_2O_3:Eu^{3+}@P(NIPAm-*co*-AAm)@HMS-FITC composites for 10 min (a–c), 30 min (d–f), and 3 h (g–i) at 37 °C. Each series can be classified to the nuclei of cells (being dyed in blue by Hoechst 33324 for visualization), Gd_2O_3:Eu^{3+}@P(NIPAm-*co*-AAm)@HMS-FITC, and a merge of the two channels of both above, respectively.

and confocal laser scanning microscope (CLSM) were used to confirm the internalization of as-prepared composite by SKOV3 cells. The sample has the potential to serve as a T_1-MR contrast agent due to the existance of Gd^{3+} ions in the composite. The multifunctional carriers exhibit a remarkable positive temperature-sensitive on–off modulation for indomethacin (IMC) release, i.e., rapid drug release rate at an increased temperature (on phase) and completely stopping at a decreased temperature (off phase). The swelling or deswelling of the hydrogel located the interstitial layer and mesochannels is believed to play a relevant role for controlled drug release. In addition, the emission intensity of Gd_2O_3:Eu^{3+} was strongly dependent with the loading and cumulative release of IMC molecules, which has potential to be used in tracking or detecting applications.

Figure 10. T_1-weighted MR imaging of various mass of Gd_2O_3:Eu^{3+}@P(NIPAm-*co*-AAm)@HMS. Deionized water (0 mg mL^{-1}) was the reference.

4. Experimental Section

Materials: *N*-isopropylacrylamide (NIPAm) was purchased from J&KCHEMICA. NIPAm monomer was recrystallized from hexane and dried in vacuum prior to use. Sodium acetate, CTAB (99%), and TEOS were purchased from Beijing Yili Fine Chemicals Co., Ltd. Diphenyl(2, 4, 6- trimethylbenzoyl)-phosphine oxide (TPO) was purchased from Tokyo Kasei Kogyo Co., Ltd. Gd_2O_3 and Eu_2O_3 (99.999%) were purchased from Science and Technology Parent Company of Changchun Institute of Applied Chemistry. FITC, acrylic acid amide (AAm), and *N*,*N*-methylenebiacrylamide (BIS) were acquired from Aladdin Company. 3-aminopropyltrimethoxysilane (APTMS) was purchased from Sigma-Aldrich. The other chemicals, including ethylene glycol, ethanol, acetone, 1, 6-dioxane, and concentrated HCl were all purchased from Beijing Chemical Regent Company.

Preparation of Hollow Mesoporous Silica Microspheres (HMS): The Fe_3O_4 spheres with a mean diameter of about 300 nm were prepared via a solvothermal method as described previously.[23] The Fe_3O_4 particles were coated with a thin silica layer generated from the hydrolysis and condensation of TEOS. Subsequently, an ordered mesoporous silica shell was coated on the Fe_3O_4@nSiO_2 surface, and the detailed procedure was described previously.[24] Fe_3O_4@nSiO_2 particles were well dispersed in a mixed solution containing CTAB (0.3 g), ethanol (60 mL), and deionized water (80 mL). Afterwards, TEOS (0.2 mL) was added dropwise to the reaction mixture under vigorous stirring and kept for 6 h at room temperature. The product was collected by centrifugation, washed with ethanol 3 times, and dried at 60 °C in vacuum. The CTAB templates were removed by the acetone extraction. Finally, the Fe_3O_4 cores were removed by acid treatment, for example by using HCl solution (2 M) at 80 °C for 8 h. The final products were named hollow mesoporous sphere (HMS).

Luminescence Functionalization of HMS by Gd_2O_3:Eu^{3+}: HMS (0.1 g) was added to a 25 mL conical flask and then vacuumed at room temperature for 0.5 h. Subsequently, an aqueous solution containing stoichiometric $Gd(NO_3)_3$ and $Eu(NO_3)_3$ was injected into the flask under magnetic stirring. The doping concentration of Eu^{3+} was 5 mol% to Gd^{3+} in Gd_2O_3:Eu^{3+}. After 0.5 h, the vacuum pump was turned off and air was allowed to refill into the system. The sample was stirred for another 12 h at ambient atmosphere and then separated by centrifugation. After drying at 100 °C for 1 h to remove water, the sample was calcined in air with a heating rate of 1 °C min^{-1} from room temperature to 550 °C, and held for 3 h for the crystallization of Gd_2O_3:Eu^{3+}. The obtained samples were denoted as Gd_2O_3:Eu^{3+}@HMS.

Synthesis of Gd_2O_3:Eu^{3+}@P(NIPAm-co-AAm)@HMS Organic–Inorganic Composite Materials: NIPAm (0.25 g), AAm (0.0157 g), BIS (0.0051 g, crosslinker), and TPO (0.0025 g, photoinitiator) were dissolved in 1,6-dioxane (1 mL) and then Gd_2O_3:Eu^{3+}@HMS (0.05 g) powders were added under vacuum similar with the previous procedure for filling Gd_2O_3:Eu^{3+} core. The suspension was further stirred overnight at room temperature in the dark, and then the resulting material was separated by centrifugation. After rinsing with 1,6-dioxane to remove the surface-adsorbed monomers and centrifugation, the monomer-containing nanoparticles were exposed to UV light (200 W cm^{-2}, LAMP, PHILIPS) for 8 min to make the photoinitiated polymerization occur. Then, the prepared product was soaked in ethanol for 12 h to remove unreacted monomers and impurities and dried in vacuum at 50 °C to obtain the final samples, denoted as Gd_2O_3:Eu^{3+}@P(NIPAm-*co*-AAm)@HMS. As for fluorescein-labeled Gd_2O_3:Eu^{3+}@P(NIPAm-*co*-AAm)@HMS,

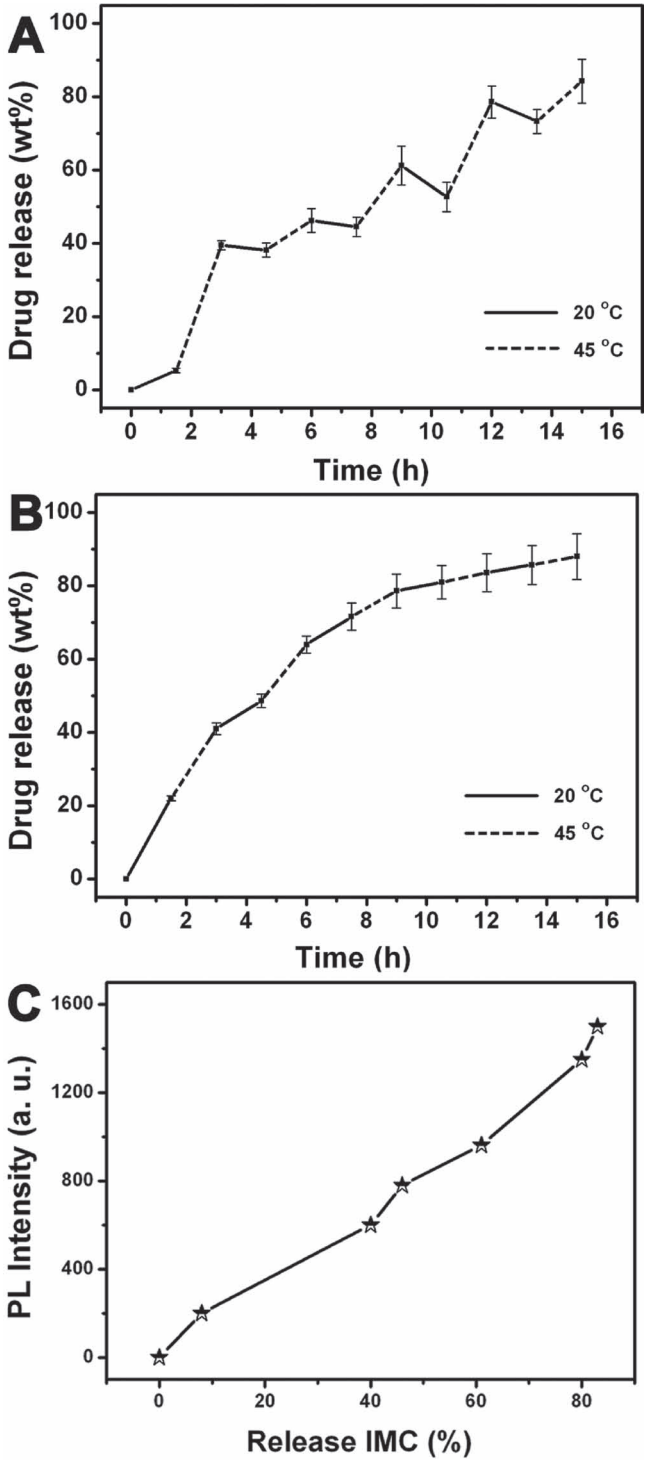

Figure 11. Controlled release of IMC from Gd_2O_3:Eu^{3+}@P(NIPAm-*co*-AAm)@HMS (A) and Gd_2O_3:Eu^{3+}@HMS (B) in response to temperature changes in 10 mM PBS (pH = 7.4). C) PL emission intensity of Eu^{3+} in Gd_2O_3:Eu^{3+}@P(NIPAm-*co*-AAm)@HMS as a function of the cumulatively released IMC.

FITC-APTMS was formed by stirring FITC in ethanolic APTMS solution overnight in the dark. Then, the dried Gd_2O_3:Eu^{3+}@P(NIPAm-*co*-AAm)@HMS sample reacted with FITC-APTMS in 30 mL of ethanol under reflux for 24 h. The resultant solid was centrifuged, washed with ethanol, and dried under vacuum.

In Vitro Cytotoxicity Assays of HMS, Gd_2O_3:Eu^{3+}@HMS and Gd_2O_3:Eu^{3+}@P(NIPAm-co- AAm)@HMS: The in vitro cytotoxicity of HMS, Gd_2O_3:Eu^{3+}@HMS and Gd_2O_3:Eu^{3+}@P(NIPAm-*co*-AAm)@HMS were determined by MTT (3-(4,5-dimethylthiazol-2-yl)-2,5-diphenyltetrazolium bromide) assays. 5000–6000 L929 fibroblast cells in 200 μL media per well were plated in 96 well plate for 24 h to allow the cells to attach, and then exposed to different concentration of HMS, Gd_2O_3:Eu^{3+}@HMS or Gd_2O_3:Eu^{3+}@P(NIPAm-*co*-AAm)@HMS (3.125, 6.25, 12.5, 25, 50, 100, and 200 μg mL^{-1}) for 24 h in 5% CO_2 at 37 °C. At the end of the incubation time, the media containing HMS, Gd_2O_3:Eu^{3+}@HMS or Gd_2O_3:Eu^{3+}@P(NIPAm-*co*-AAm)@HMS was removed, and then the MTT solution (20 μL, diluted in a culture medium to a final concentration of 5 mg mL^{-1}) was added. After incubation at 37 °C in the dark for 4 h, 100 μL of acidified isopropanol was added to each well, and the absorbance was monitored with a microplate reader at a wavelength of 570 nm. Averages and standard deviations were based on four samples and all tests performed in triplicate. The cell viability was calculated using the following equation: Cell viability (%) = $[A]_{test}/[A]_{control} \times 100$, where $[A]_{test}$ is the average cell viability after adding as-prepared Gd_2O_3:Eu_3+@P(NIPAm-*co*-AAm)@HMS nanoparticles and $[A]_{control}$ is the cell viability for the control experiment that did not add nanoprticles.

Cell Uptake: Cellular uptake by SKOV3 ovarian cancer cells was examined using flow cytometry and CLSM, respectively. For flow cytometry studies, SKOV3 ovarian cancer cells (1×10^5) were seeded in 6-well culture plates and grown overnight. The cells were then treated with Gd_2O_3:Eu^{3+}@P(NIPAm-*co*-AAm)@HMS-FITC or free FITC at 37 °C for 10 min, 30 min, and 3 h, respectively. A single cell suspension was prepared consecutively by trypsinization, washing with PBS, and filtration through 35 mm nylon mesh. Thereafter, the cells were lifted using a cell stripper (Media Tech. Inc.) and analyzed using a flow ctyometer (FACSCalibur). Cells incubated in the absence of the microspheres were used as the control.

For CLSM, the SKOV3 ovarian cancer cells were seeded in 6-well culture plates (a clean cover slip was put in each well) and grown overnight as a monolayer, and were incubated with Gd_2O_3:Eu^{3+}@P(NIPAm-*co*-AAm)@HMS-FITC at 37 °C for 10 min. Thereafter, the cells were rinsed with PBS three times, fixed with 2.5% formaldehyde (1 mL per well) at 37 °C for 10 min, and then rinsed with PBS three times again. For nucleus labeling, the nuclei were stained with Hoechst 33342 solution (from Molecular Probes, 20 mg mL^{-1} in PBS, 1 mL per well) for 10 min and then rinsed with PBS three times. The cover slips were placed on a glass microscope slide, and the samples were visualized using CLSM (FV10-ASW).

In Vitro MR Assay: The T_1-weighted MR images were obtained using a 1.5 T Siemens Magnetom Espree. Dilutions of Gd_2O_3:Eu^{3+}@P(NIPAm-*co*-AAm)@HMS samples (0.75, 0.5, 0.25, 0.1, 0.025 mg mL^{-1}) in deionized water were placed in a series of 2 mL tubes for T_1-weighted MR imaging. The following parameters were adopted: TR/TE (repetition time/echo time) = 500/9.5 ms, matrix = 512 × 512, FOV (field of view in cm) = 350 × 350, slice thickness = 3.0 mm.

In Vitro Indomethacin (IMC) Loading and Release Test: IMC was selected as the model drug for release test. Typically, the composite (0.1 g) was immersed in 10 mL of ethanol-water (4:1, v/v) solution with IMC concentration of 16 mg mL^{-1}, and soaked for 24 h with stirring. The IMC-loaded Gd_2O_3:Eu^{3+}@P(NIPAm-*co*-AAm)@HMS was separated by centrifugation and dried at 80 °C for 12 h. The loading amount of IMC was determined by thermogravimetry (TG) analysis.

A certain amount of IMC-loaded Gd_2O_3:Eu^{3+}@P(NIPAm-*co*-AAm)@HMS was immersed in 5 mL of phosphate buffer solution (pH 7.4 PBS, 10 mM). At certain time intervals and different temperature, aliquots of PBS supernatant (100 μL) were taken out after centrifugation to test the concentration of the released IMC by UV-vis absorption spectra (monitored on 320 nm) and 100 μL fresh PBS was added to the tube again for the continued drug release.

Characterization: XRD was performed on a D8 Focus diffractometer (Bruker) with Cu Kα radiation (λ = 0.15405 nm). FTIR spectra were recorded on a Perkin-Elmer 580BIR spectrophotometer using KBr

pellet technique. N_2 adsorption/desorption isotherms were obtained on a Micromeritics ASAP 2020 M apparatus. Pore size distribution was calculated from the adsorption branch of N_2 adsorption/desorption isotherm and the Barret–Joner–Halenda (BJH) method. The BET surface areas were determined using the data between 0.05 and 0.35 just before the capillary condensation, and the pore volume was obtained by the t-plot method. TG measurements (Netzsch Thermoanalyzer STA 409) were used to determine the loading amount of indomethacin on the materials in an atmospheric environment with a heating rate of 10 °C min^{-1} from room temperature to 800 °C. The morphology and composition of the samples were inspected using FESEM (XL30, Philips) equipped with an energy-dispersive X-ray spectrum (EDS, JEOL JXA-840). TEM images were recorded on a FEI Tecnai G2 S-Twin transmission electron microscope with a field emission gun operating at 200 kV. Elemental mapping was conducted using the TEM equipped with an energy dispersive X-ray spectroscope (EDX). The PL measurements were performed with a Hitachi F-7000 spectrophotometer equipped with a 150 W xenon lamp as the excitation source. The UV-vis absorption spectra values were measured on a TU-1901 spectrophotometer. Flow cytometry analysis was performed on FACSCalibur flow cytometer (BD Biosciences) with 488 nm excitation lasers. CLSM images were observed by confocal laser scanning microscope (Olympus, FV 1000).

Supporting Information

Supporting Information is available from the Wiley Online Library or from the author.

Acknowledgements

This project was financially supported by National Basic Research Program of China (2010CB327704), National High Technology Program of China (2011AA03A407), and the National Natural Science Foundation of China (NSFC 51172228, 21101149, 51172227, 20921002).

Received: November 14, 2011
Published online: January 30, 2012

[1] a) H. C. Guo, H. S. Qian, S. Q. Sun, D. H. Sun, H. Yin, X. P. Cai, Z. X. Liu, J. Y. Wu, T. Jiang, X. T. Liu, *Chem. Cent. J.* **2011**, *5*, 1; b) Y. F. Zhu, J. L. Shi, W. H. Shen, X. P. Dong, J. W. Feng, M. L. Ruan, Y. S. Li, *Angew. Chem. Int. Ed.* **2005**, *44*, 5083; c) Y. F. Zhu, J. L. Shi, W. H. Shen, H. R. Chen, X. P. Dong, M. L. Ruan, *Nanotechnology* **2005**, *16*, 2633; d) X. M. Jiang, T. L. Ward, Y. S. Cheng, J. W. Liu, C. J. Brinker, *Chem. Commun.* **2010**, *46*, 3019; e) Y. Zhao, L. N. Lin, Y. Lu, S. F. Chen, L. Dong, S. H. Yu, *Adv. Mater.* **2010**, *22*, 5255; f) C. C. Huang, W. Huang, C. S. Yeh, *Biomaterials* **2011**, *32*, 556; g) J. G. Wang, H. J. Zhou, P. C. Sun, D. T. Ding, T. H. Chen, *Chem. Mater.* **2009**, *21*, 612; h) S. H. Han, W. G. Hou, J. Xu, Z. M. Li, *Colloid Polym. Sci.* **2004**, *282*, 1286; i) N. Venhatathri, *Mater. Sci. Eng., C* **2008**, *28*, 1260; j) J. Liu, S. B. Hartono, Y. G. Jin, Z. Li, G. Q. Lu, S. Z. Qiao, *J. Mater. Chem.* **2010**, *20*, 4595; k) J. H. Wu, X. S. Li, Y. Zhao, Q. Gao, L. Guo, Y. Q. Feng, *Chem. Commun.* **2010**, *46*, 9031.

[2] Y. F. Zhu, Y. Fang, S. Kaskel, *J. Phys. Chem. C* **2010**, *114*, 16382.

[3] a) P. P. Yang, Z. W. Quan, C. X. Li, H. Z. Lian, S. S. Huang, J. Lin, *Microporous Mesoporous Mater.* **2008**, *116*, 524; b) P. P. Yang, Z. W. Quan, S. S. Huang, J. Lin, *Biomaterials* **2008**, *29*, 692; c) F. Wang, X. G. Liu, *Chem. Soc. Rev.* **2009**, *38*, 976; d) F. Wang, D. Banerjee, Y. S. Liu, X. Y. Chen, X. G. Liu, *Analyst* **2010**, *135*, 1839; e) Z. H. Xu, C. X. Li, P. A. Ma, Z. Y. Hou, D. M. Yang, X. J. Kang, J. Lin, *Nanoscale* **2011**, *3*, 661; f) J. Shen, L. D. Sun, J. D. Zhu, L. H. Wei, H. F. Sun, C. H. Yan, *Adv. Funct. Mater.* **2010**, *20*, 3708; g) P. Ghosh, E. de la Rosa, J. Oliva, D. Solis, A. Kar, A. Patra, *J. Appl. Phys.* **2009**, *105*, 113532; h) P. Ghosh, A. Kar, A. Patra, *Nanoscale* **2010**, *2*, 1196; i) D. J. Naczynski, T. Andelman, D. Pal, S. Chen, R. E. Riman, C. M. Roth, P. V. Moghe, *Small* **2010**, *6*, 1631; j) Z. W. Quan, J. Y. Fang, *Nano Today* **2010**, *5*, 390; k) Z. W. Quan, D. M. Yang, P. P. Yang, X. M. Zhang, H. Z. Lian, X. M. Liu, J. Lin, *Inorg. Chem.* **2008**, *47*, 9509; l) A. K. Sharma, K. H. Son, B. Y. Han, K. S. Sohn, *Adv. Funct. Mater.* **2010**, *20*, 1750; m) D. T. Tu, L. Q. Liu, Q. Ju, Y. S. Liu, H. M. Zhu, R. F. Li, X. Y. Chen, *Angew. Chem. Int. Ed.* **2011**, *50*, 6306; n) Y. S. Liu, D. T. Tu, H. M. Zhu, R. F. Li, W. Q. Luo, X. Y. Chen, *Adv. Mater.* **2010**, *22*, 3266; o) W. Q. Luo, C. Y. Fu, R. F. Li, Y. S. Liu, H. M. Zhu, X. Y. Chen, *Small* **2011**, *7*, 3046; p) Y. H. Wang, Y. S. Liu, Q. B. Xiao, H. M. Zhu, R. F. Li, X. Y. Chen, *Nanoscale* **2011**, *3*, 3164.

[4] a) H. Wang, J. Yang, C. M. Zhang, J. Lin, *J. Solid State Chem.* **2009**, *182*, 2716; b) L. Q. Liu, E. Ma, R. F. Li, G. K. Liu, X. Y. Chen, *Nanotechnology* **2007**, *18*, 015403; c) L. F. Hu, R. Z. Ma, T. C. Ozawa, T. Sasaki, *Angew. Chem. Int. Ed.* **2009**, *48*, 3846; d) D. H. Park, S. H. Cho, J. S. Kim, K. S. Sohn, *J. Alloys Compd.* **2008**, *449*, 196; e) J. Yang, C. X. Li, Z. Y. Cheng, X. M. Zhang, Z. W. Quan, C. M. Zhang, J. Lin, *J. Phys. Chem. C* **2007**, *111*, 19148; f) L. Q. Liu, E. Ma, R. F. Li, X. Y. Chen, *J. Nanosci. Nanotechnol.* **2008**, *8*, 1398; g) L. Q. Liu, X. Y. Chen, *Nanotechnology* **2007**, *18*, 255704; h) F. Wang, R. R. Deng, J. Wang, Q. X. Wang, Y. Han, H. M. Zhu, X. Y. Chen, X. G. Liu, *Nat. Mater.* **2011**, *10*, 968.

[5] a) I.-F. Li, C.-H. Su, H.-S. Sheu, H.-C. Chiu, Y.-W. Lo, W.-T. Lin, J.-H. Chen, C.-S. Yeh, *Adv. Funct. Mater.* **2008**, *18*, 766; b) J. Zhou, M. X. Yu, Y. Sun, X. Z. Zhang, X. J. Zhu, Z. H. Wu, D. M. Wu, F. Y. Li, *Biomaterials* **2011**, *32*, 1148; c) J. Zhou, Y. Sun, X. X. Du, L. Q. Xiong, H. Hu, F. Y. Li, *Biomaterials* **2010**, *31*, 3287; d) Q. Ju, Y. S. Liu, D. T. Tu, H. M. Zhu, R. F. Li, X. Y. Chen, *Chem. Eur. J.* **2011**, *17*, 8549.

[6] a) W. R. Zhao, H. R. Chen, Y. S. Li, M. D. Lang, J. L. Shi, *Adv. Funct. Mater.* **2008**, *18*, 2780; b) K. Kamata, Y. Lu, Y. N. Xia, *J. Am. Chem. Soc.* **2003**, *125*, 2384; c) L. Sun, Y. Zang, M. D. Sun, H. G. Wang, X. J. Zhu, S. F. Xu, Q. B. Yang, Y. X. Li, Y. M. Shan, *J. Colloid Interface Sci.* **2010**, *350*, 90.

[7] a) Q. Yang, S. C. Wang, P. W. Fan, L. F. Wang, Y. Di, K. F. Lin, F.-S. Xiao, *Chem. Mater.* **2005**, *17*, 5999; b) Q. Gan, X. Y. Lu, J. C. Qian, H. J. Zhou, X. Lu, J. L. Shi, C. S. Liu, *Biomaterials* **2011**, *32*, 1932; c) Y. J. Jing, Y. H. Zhu, X. L. Yang, J. H. Shen, C. Z. Li, *Langmuir* **2011**, *27*, 1175; d) N. A. Peppas, W. Leobandung, *J. Biomater. Sci. Polym. Ed.* **2004**, *15*, 125.

[8] a) Y. Shin, J. Liu, J. H. Chang, G. J. Exarhos, *Chem. Commun.* **2002**, *16*, 1718; b) H. M. N. El-Din, *J. Appl. Polym. Sci.* **2011**, *119*, 577; c) H. K. Fu, S. W. Kuo, F. C. Huang, F. C. Chang, H. C. Lin, *Polymer* **2009**, *50*, 1246; d) J. Guo, W. L. Yang, Y. H. Deng, C. C. Wang, S. K. Fu, *Small* **2005**, *1*, 737.

[9] Z. Z. Yin, J. J. Zhang, L. P. Jiang, J. J. Zhu, *J. Phys. Chem. C* **2009**, *113*, 16104.

[10] G. Fundueanu, M. Constantin, P. Ascenzi, *Int. J. Pharm.* **2009**, *379*, 9.

[11] a) H. G. Schild, *Prog. Polym. Sci.* **1992**, *17*, 163; b) Y. Qiu, K. Park, *Adv. Drug. Delivery Rev.* **2001**, *53*, 321.

[12] G. R. Hendrickson, M. H. Smith, A. B. South, L. A. Lyon, *Adv. Funct. Mater.* **2010**, *20*, 1697.

[13] a) C. S. Brazel, *Pharm. Res.* **2009**, *26*, 644; b) N. S. Satarkar, J. Z. Hilt, *J. Controlled Release* **2008**, *130*, 246; c) T. Fujigaya, T. Morimoto, Y. Niidome, N. Nakashima, *Adv. Mater.* **2008**, *20*, 3610; d) B. P. Timko, T. Dvir, D. S. Kohane, *Adv. Mater.* **2010**, *22*, 4925; e) S. R. Sershen, S. L. Westcott, N. J. Halas, J. L. West, *Appl, Phys. Lett.* **2002**, *80*, 4609; f) W. Y. Li, X. Cai, C. H. Kim, G. R. Sun, Y. Zhang, R. Deng, M. X. Yang, J. Y. Chen, S. Achilefu, L. H. V. Wang, Y. N. Xia, *Nanoscale* **2011**, *3*, 1724.

[14] a) Y. Z. You, K. K. Kalebaila, S. L. Brock, D. Qupický, *Chem. Mater.* **2008**, *20*, 3354; b) J. Guo, W. L. Yang, C. C. Wang, J. He, J. Y. Chen, *Chem. Mater.* **2006**, *18*, 5554; c) C. Y. Liu, W. L. Yang, J. H. Hu, C. C. Wang, S. K. Fu, *J. Mater. Chem.* **2009**, *19*, 7464; d) C. Y. Hong, X. Li, C. Y. Pan, *J. Phys. Chem. C* **2008**, *112*, 15320.

[15] a) X. Z. Zhang, R. X. Zhuo, J. Z. Cui, J. T. Zhang, *Int. J. Pharm.* **2002**, *235*, 43; b) Y. S. Shin, J. H. Chang, J. Liuc, R. Williforda, Y. K. Shin, G. J. Exarhos, *J. Controlled Release* **2001**, *73*, 1.

[16] a) Z. Y. Zhou, S. M. Zhu, D. Zhang, *J. Mater. Chem.* **2007**, *17*, 2428; b) B. S. Tian, C. Yang, *J. Phys. Chem. C* **2009**, *113*, 4925; c) V. Lapeyre, N. Renaudie, J. F. Dechezelles, H. Saadaoui, S. Ravain, V. Ravaine, *Langmuir* **2009**, *25*, 4659; d) K. Suzuki, T. Yumura, Y. Tanaka, M. Akashi, *J. Controlled Release* **2001**, *75*, 183; e) J. Shi, L. H. Liu, X. P. Liu, X. M. Sun, S. K. Cao, *Polym. Adv. Technol.* **2008**, *19*, 1467; f) L. M. Geever, C. L. Higginbotham, *J. Mater. Sci.* **2011**, *46*, 3233; g) M. Bikram, A. M. Gobin, R. E. Whitmire, J. L. West, *J. Controlled Release* **2007**, *123*, 219; h) Y. F. Zhu, S. Kaskel, T. Ikoma, N. Hanagata, *Microporous Mesoporous Mater.* **2009**, *123*, 107.

[17] Y. Chen, J. O. Iroh, *Chem. Mater.* **1999**, *11*, 1218.

[18] P. J. Kooyman, M. J. Verhoef, E. Prouzet, *Stud. Surf. Sci. Catal.* **2000**, *129*, 535.

[19] M. L. Pang, J. Lin, R. B. Xing, C. X. Luo, Y. C. Han, *Opt. Mater.* **2003**, *23*, 547.

[20] a) M. S. Yavuz, Y. Y. Cheng, J. Y. Chen, C. M. Cobley, Q. Zhang, M. Rycenga, J. W. Xie, C. H. Kim, K. H. Song, A. G. Schwartz, L. H. V. Wang, Y. N. Xia, *Nat. Mater.* **2010**, *8*, 935; b) R. Yoshida, K. Sakai, T. Okano, Y. Sakurai, *J. Biomater. Sci., Polym. Ed.* **1995**, *6*, 595; c) J. Chen, K. Park, *Pure Appl. Chem.* **1999**, *A36*, 917.

[21] a) H. B. Du, R. Wickramasinghe, X. H. Qian, *J. Phys. Chem. B* **2010**, *114*, 16594; b) M. Taha, B. S. Gupta, I. Khoiroh, M. J. Lee, *Macromolecules* **2011**, *44*, 8575.

[22] a) G. Blasse, *Prog. Solid State Chem* **1988**, *18*, 79; b) M. F. H. Schuurmans, J. M. F. Van Dijk, *Physica B&C* **1984**, *123*, 131.

[23] H. Deng, X. L. Li, Q. Peng, X. Wang, J. P. Chen, Y. D. Li, *Angew. Chem. Int. Ed.* **2005**, *44*, 2782.

[24] Y. H. Deng, D. W. Qi, C. H. Deng, X. M. Zhang, D. Y. Zhao, *J. Am. Chem. Soc.* **2008**, *130*, 28.